*Meteoritics & Planetary Science* 41, Nr 4, 571–580 (2006)
Abstract available online at http://meteoritics.org

# TEM studies and the shock history of a "mysterite" inclusion from the Krymka LL chondrite

I. WEBER[1*], V. P. SEMENENKO[2], T. STEPHAN[1], and E. K. JESSBERGER[1]

[1]Institute for Planetology and Interdisciplinary Center for Electron Microscopy and Microanalysis, Westfälische Wilhelms-Universität Münster, Wilhelm-Klemm-Str. 10, 48149 Münster, Germany
[2]Institute of Environmental Geochemistry, NAS of Ukraine, Palladina 34a, Kyiv-142, 03180, Ukraine
*Corresponding author. E-mail: sonderm@uni-muenster.de

*(Received 28 June 2004; revision accepted 09 December 2005)*

**Abstract**–The microstructure and composition of the matrix of one carbonaceous inclusion (K1) in the Krymka LL3.1 chondrite were studied using transmission electron microscopy (TEM). K1 has previously shown an enigmatic nature and similarities with volatile-rich, fine-grained, dark inclusions of Krymka called "mysterite."

In the present study, four minerals were identified by TEM. Olivine, pyroxene, and pyrrhotite typically have grain sizes of one micrometer; graphite occurs as flakes of a similar size. Olivine shows a moderately high dislocation density most probably caused by shock. Pyroxene shows coexisting ortho- and clinoenstatite lamellae that probably originated from shear stress after a shock event or from the rapid cooling of the protoenstatite stability field. However, we demonstrate that in this case, a shock trigger is more likely. Pyrrhotite in the studied sample occurs as a 4C monoclinic superstructure. The graphite flakes in the fragment are well crystallized, as can be seen by discrete spots in the diffraction pattern. In graphite, the degree of crystallization increases with the metamorphic grade. Based on the microstructure of this mineral we conclude that after a first moderate shock event, the residual temperature between 300 °C and 500 °C led to thermal metamorphism. A second shock event, possibly at excavation from the parent body, is responsible for the shock features observed in olivine, pyroxene, and graphite.

## INTRODUCTION

Krymka, one of the most primitive ordinary chondrites, fell to the Earth as a shower of rocks on January 21, 1946. About 25 kg of material was collected immediately after it fell in the Nikolaev region of the Ukraine. An additional 25 kg of material has since been collected (Dreizin 1958). The Krymka meteorite is an unequilibrated gas-rich fragmental breccia classified as a LL3.1 chondrite with a shock stage of S3, which corresponds to shock pressures in the range of 5–20 GPa (Stöffler et al. 1991). Studies of many individual samples of the Krymka host indicate abundant evidence of shock transformation of the chondritic material, ranging from samples without visible shock effects to samples containing completely shock-melted regions (Semenenko et al. 1987; Semenenko and Perron 1995). In addition, shock-melted regions of the Krymka sample #1290/29 contain evidence of mechanical deformations (shear deformations of some phosphate globules and troilite grains), which indicate at least one additional, although less intensive, shock after solidification of the shock melts in the chondritic material (Semenenko and Perron 1995).

Krymka is characterized by the occurrence of a high modal abundance of xenolithic clasts (Semenenko and Girich 2001; Semenenko et al. 2001). These fine-grained foreign inclusions are dominated by carbonaceous clasts, which are of extraordinary scientific interest.

This very rare, fine-grained, dark material has so far been discovered only in two meteorites, Krymka (LL3.1) and Supuhee (H6). Laul et al. (1973) detected an enrichment of Ag, Tl, and Bi in these two ordinary chondrites. They concluded that this enrichment has its origin in an admixture of a phase rich in these elements in a late condensate introduced during a brecciation event. Since the petrographic carrier of the volatiles could not be specified, they named this material "mysterite." Higuchi et al. (1977) studied four mysterite fragments from the H6 chondrite Supuhee by radiochemical neutron activation, and Grossman et al. (1980) investigated a mysterite-bearing inclusion from the Krymka LL3.1 chondrite with an electron microprobe. Although they

used very different analytical techniques, both groups concluded that mysterite belongs to an unknown kind of carbonaceous material (Higuchi et al. 1977; Grossman et al. 1980). The inclusion is made of a fine-grained mixture of silicates and FeS (here identified as troilite, e.g., Semenenko et al. 2005) and, in addition, coarse grains of pyroxene, olivine, and rare metal particles.

In addition to these investigations, Campins and Swindle (1998) speculated on the basis of results from the Halley missions (summarized in Jessberger 1999) that among all known types of meteoritic and xenolithic material the carbonaceous xenoliths from Krymka and Supuhee are the candidates most likely to have been of cometary origin.

Two clasts (K1 and K2) of this unknown carbonaceous material from Krymka with similar mineralogy were studied by Semenenko et al. (1991) and Semenenko (1996). All of the inclusions are characterized by a bulk composition similar to C2 chondrites. However, graphite is also present. The presence of microcrystals of graphite, heterogeneous and slightly metamorphosed minerals, and an anomalous enrichment of Ag and Zn are the most distinctive features of the inclusion K1. It was inferred that its graphite was formed from organic compounds as a result of metamorphism. In addition to graphite crystals, there are also C-rich areas of unknown material and organic compounds (Semenenko et al. 2005). The spatial concentration of certain ion species (such as $H^-$, $C^-$, $CH^-$, $C_2^-$, and $C_2H^-$; Semenenko et al. 2005), measured with time-of-flight secondary ion mass spectrometry, are visible in black areas in scanning electron microscopy (SEM) images. The C-rich areas suggest that they are composed of not graphitized or poorly graphitized material, which most likely represents a transitional state from organic compounds to graphite caused by a metamorphic process (Semenenko 1996; Semenenko and Girich 1996).

In a combined analytical study (Semenenko et al. 2003, 2005), a detailed examination of one polished small splinter (1.5 × 1.5 mm) of the Krymka carbonaceous clast K1 was carried out using reflected light microscopy, SEM, secondary ion mass spectrometry, and transmission electron microscopy (TEM). The mineralogical, chemical, and isotopic features, as well as the nature of the graphite and other minerals, were investigated to obtain information on their mineral associations with the aim of finding conclusive evidence concerning the origin of mysterite, a material that had already been associated with comets. The results of these combined investigations allow the following conclusions: the xenolith formation is a result of the accretion of heterogeneous components in a region depleted in chondrules. After this process, which was followed by lithification and a probable collisional fragmentation of a primary carbonaceous body, this xenolith and some others (Semenenko et al. 2005) were covered with extremely fine-grained silicate dust. Together with the main Krymka constituents, the xenoliths were accreted in the Krymka parent body. It is not clear whether the metamorphic processes occurred within this parent body or on the primary body (Semenenko et al. 2005).

In addition to these conclusions made by Semenenko et al. (2005), this study presents the results from more extensive structural TEM analyses of the matrix of the Krymka carbonaceous clast K1. TEM was used to gather information about the microstructure of the matrix minerals, especially the stage of crystallinity of graphite, and therefore about the metamorphic history of the clast and the Krymka parent body itself.

## SAMPLE SELECTION AND PREPARATION

The main mass (~26 kg) of the Ukrainian meteorite Krymka belongs to the meteorite collection of the Museum of Natural History, National Academy of Science (NAS) of Ukraine, Kyiv. The Krymka sample investigated in this study, including carbonaceous clast K1 (Figs. 1a and 1b), also stems from this collection. Mineralogical and chemical examinations of the interesting fragment were already performed in Kyiv and Moscow (Semenenko et al. 1991) as well as in Paris (Semenenko 1996). Locally anomalous enrichment of Ag and Zn and the overall composition of approximately 90 vol% matrix that contains a uniform fine-grained mixture of olivine, pyroxene, FeS (here identified as troilite, e.g., Semenenko et al. 2005), graphite, Fe,Ni metal, and some minor minerals indicated that K1 is most likely a mysterite clast. Other textural components in K1 are chondrules or their fragments, coarse olivine grains, and an amoeboid olivine grain (Semenenko et al. 1991; Semenenko et al. 2005).

An ~1.5 × 1.5 mm and 200 μm thick polished section of the clast K1 was prepared for the combined analytical study (Fig. 1b). A detailed analytical, mineralogical, and petrographic description of exactly this sample of K1 was provided by Semenenko et al. (2003, 2005).

To obtain an ~100 nm thin foil from this thick section for TEM analyses, the focused ion beam (FIB) technique was used (Giannuzzi and Stevie 1999; Stevie et al. 2001; Hutchinson et al. 2003). During the last few years, this tool has become increasingly important for the preparation of TEM specimens. An ion beam from a gallium liquid metal ion source is used to cut an extremely thin slice out of a thicker section. Gallium ions irradiate a pre-determined sample position ~15 μm in length and ~10 μm in depth from both sides until an ~100 nm thin section has been produced. A strong current ion beam was used to produce a first rough slice, from which the final precise specimen was cut using an extremely fine (<10 nm in diameter) ion beam. The sample that was prepared was extracted from the substrate by first cutting along the bottom and then cutting along both sides with the ion beam. The position of the sample within the K1 fragment can be seen in Fig. 1c. The

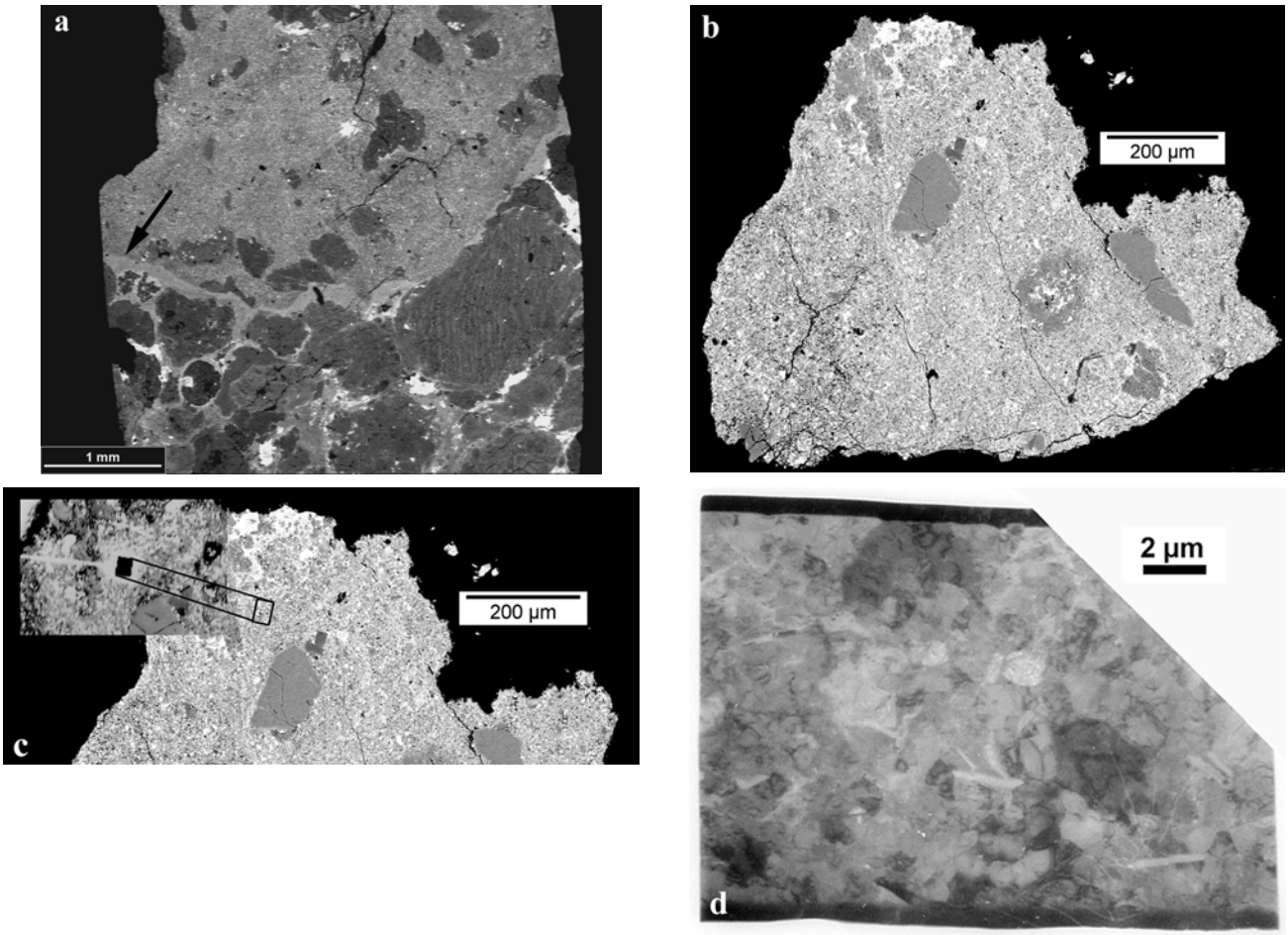


Fig. 1. a) A portion of the xenolith with a thin, fine-grained rim of light gray color (arrow) in contact with the meteorite host (lower part of the figure). The xenolith consists of fine-grained matrix, rare chondrules and their fragments, and coarse grains (BSE image). b) An SEM image of the inner part of the fine-grained carbonaceous clast K1 already visible at the top in (a), which is prepared for detailed investigation (BSE image). c) A cutout of the SEM image shown in (b), in which the selected area is marked. In the transmitted light image (upper left corner) the hole produced by the ion beam is visible. d) A TEM bright field image of the thin foil produced with the ion beam. Already visible is the extremely fine-grained occurrence of the single grains, and, in addition, some graphite laths. More details in relation to images (a) and (b) are given in Semenenko et al. (2005).

thin foil obtained is shown in Fig. 1d. For the TEM investigations, which were performed with a JEOL JEM-3010 instrument operating at 300 kV, the thin section was positioned on a carbon-coated copper grid. All quantitative analyses of the examined minerals were obtained with a Pentafet X-ray detector (Oxford Instruments) for energy dispersive analysis (EDS, Link ISIS). Theoretical k factors (given by Oxford Instruments), which were scrutinized by using suitable mineral standards, were used for element standardization.

## RESULTS

The fine-grained xenolith K1 was found in an individual Krymka sample. The hand sample shows a dark compact clast with a sharp boundary to the Krymka host, which is also visible in the SEM overview in Fig. 1a. The xenolith consists of three main textural components: a uniform fine-grained matrix, a small number of chondrules or their fragments, and a very few coarse grains.

In the present study, TEM analyses of the matrix of the carbonaceous clast K1 revealed that the thin section investigated contains olivine, pyroxene, graphite, and an FeS phase. These phases, except graphite, were quantitatively analyzed with EDS. The results are given in Table 1.

### Olivine

The main matrix mineral, olivine, which has an average grain size of 1 µm, is also abundant in this specimen. Previous TEM investigations (Weber et al. 2003) showed no significant indications suggestive of a high dislocation density (Fig. 2a). Further TEM studies with a different tilting angle, however, confirm the occurrence of numerous dislocations with

Table 1. Chemical composition of minerals in the carbonaceous clast K1 of the LL chondrite Krymka.

| | Olivine | | | | Pyroxene | | Pyrrhotite |
|---|---|---|---|---|---|---|---|
| O | 58.7 | 55.5 | 58.0 | 58.0 | 59.9 | 60.4 | |
| Mg | 17.0 | 17.5 | 19.4 | 23.1 | 16.8 | 16.2 | |
| Si | 14.8 | 14.8 | 15.1 | 14.3 | 20.1 | 20.5 | |
| Ca | | | | | 0.21 | 0.14 | |
| Fe | 9.4 | 12.2 | 7.5 | 4.6 | 3.0 | 2.8 | 47.0 |
| S | | | | | | | 53.0 |
| Total | 99.9 | 100.0 | 100.0 | 100.0 | 100.01 | 100.04 | 100.0 |
| En | | | | | 84 | 85 | |
| Fs | | | | | 15 | 15 | |
| Wo | | | | | 1 | | |
| Fo | 64 | 59 | 72 | 83 | | | |
| Fa | 36 | 41 | 28 | 17 | | | |

Data in atom% and mole%; analyses are normalized to 100%.

Burgers vector [001] (Fig. 2b). To estimate the dislocation density, we counted the number of lines that interact with the foil surface (Hirsch et al. 1965). The number of lines threading the silicate is approximately $2.3 \times 10^{12}$ lines/cm$^2$. A high dislocation density with Burgers vector *c* has been observed in shocked meteorites (Madon and Poirier 1983; Langenhorst and Greshake 1999) and experimentally shocked olivine (Langenhorst et al. 1999). In addition, dislocations in olivine would also be expected from a meteorite classified as S3, which means a shock pressure of up to 20 GPa (Stöffler et al. 1991). EDS analyses of four olivine grains revealed a forsterite content of 83 mole% and below (Table 1). Previous SEM-EDS examinations of the K1 thin section revealed olivine data in a range of $Fo_{54.3}$–$Fo_{78}$ (Semenenko et al. 2005).

**Pyroxene**

TEM studies of pyroxenes revealed the same grain size of 1 μm for these minerals as for olivine. EDS analyses given in Table 1, show the occurrence of a pyroxene with $En_{84–85}$. Former SEM-EDS analyses of different pyroxenes in the matrix of K1 yield a range of $En_{82–65}Wo_{0–7}$. Only one Ca-rich pyroxene was found with a composition of $En_{57}Wo_{15}$ (Semenenko et al. 2005). Only one type of defect on TEM scale was found in pyroxene: transformation lamellae due to translational gliding (slip) along the (100) plane parallel to [001] (Figs. 3a and 3b). The corresponding electron diffraction pattern (SAED) of areas with high incidence of these lamellae shows a strong streaking of spots along the reciprocal a* direction, indicating an intergrowth of two polymorphs (Fig. 3a, insert). In the case of pyroxene, an ortho-/clinoenstatite inversion is responsible for a streaking. The more precise high-resolution TEM (HRTEM) image shows the occurrence of orthopyroxene lamellae next to clinopyroxene lamellae (Fig. 3c). Lattice fringes parallel to (100) of clinopyroxene are identified by 9 Å lattice spacing, whereas the doubled 18 Å lattice spacing corresponds to the orthopyroxene lamellae.

**Graphite**

Graphite pervades the sample as lamellae crystals or flakes ~100 × 400 nm in size (Fig. 4a). At the TEM scale, it is observable that some flakes broke up into two laths. Other graphite crystals show a kinking within one flake (Fig. 4b). The SAED pattern of the flake in Fig. 4a (insert) shows discrete spots, reflecting the well-developed crystalline character of this material. The HRTEM image of graphite (Fig. 4c) shows a region where short discontinuous fringes are visible. The distance between the fringes $d_{002}$ is ~3.4 Å as expected for crystallized graphite.

**FeS Phase**

FeS is a rare phase in this section. The located grains occur with a size of approximately 1 μm (Fig. 5a). Because of an iron content of 47 atom%, this FeS phase could be identified as pyrrhotite with $Fe_7S_8$ (Table 1). Concerning the composition, it is easier to distinguish between troilite and pyrrhotite, but the microstructure of both phases is much more complex. For pyrrhotite itself, two structural types, a monoclinic and a hexagonal type, have been found in natural specimens (Carpenter and Desborough 1964). Furthermore, a variety of superstructures are known for this phase (Buseck 1974; Dodony and Posfai 1990; Posfai and Dodony 1990). For an $Fe_7S_8$ pyrrhotite, a 4C monoclinic superstructure was observed by Nakazawa et al. (1975), which fits with our investigation of Krymka. The corresponding diffraction pattern (Fig. 5b) of the studied pyrrhotite identifies it as a superstructured monoclinic phase. The HRTEM image of another pyrrhotite (Fig. 5c) shows well-ordered lattice fringes over a long range of lattices.

## DISCUSSION

The detailed TEM study of a fine-grained, graphite-bearing carbonaceous matrix of the Krymka xenolith K1 enabled us to obtain essential data on thermal and shock

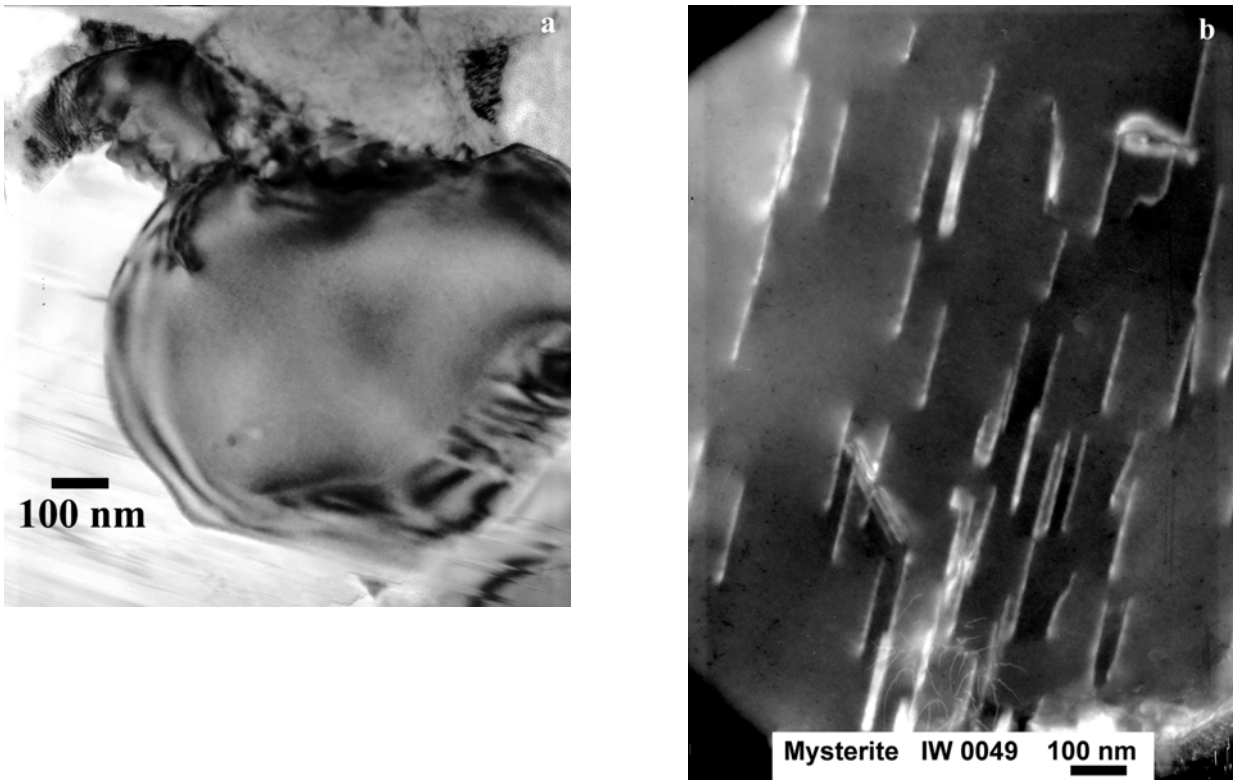


Fig. 2. a) A TEM bright field image of an ~1 µm olivine grain surrounded by pyroxene on the left and pyrrhotite in the upper right corner. b) A TEM weak beam image of an olivine grain with a high density of dislocations (white lines).

history of the xenolith itself and of the chondritic parent body.

**Olivine**

Olivine in the investigated thin foil shows a relatively high dislocation density, as usual for meteorites shocked with a pressure of up to 20 GPa. Experimental studies and examinations of naturally deformed olivine prove this assumption (Langenhorst et al. 1999; Langenhorst and Greshake 1999). This kind of dislocation is mostly of a screw character with the Burgers vector *c*. The Burgers vector gives the direction of the deformation that is associated with a dislocation within the crystal. Dislocations in olivine are typically generated at planar fractures, which also arise at this weak shock stage (starting at shock pressures of ~4–5 GPa). Although the highest forsterite content of the TEM-EDS analyses is higher than the highest forsterite value of the SEM-EDS analyses, the overall range is equal. Furthermore, this data conforms with olivine (average of Fo ~81 mole%) values of matrix from Krymka published by Weisberg et al. (1997).

**Pyroxene**

For enstatite, it is conspicuous that a twinning on (100) of the clinoenstatite, as otherwise frequently observed in shocked meteorites (Müller 1993), could not unequivocally be proven in the diffraction pattern with the observed direction. However, transformation lamellae due to a shearing along the (100) glide plane are visible. The SAED pattern and the HRTEM image (with $d_{100,oen}$ ~18 Å and ½ $d_{100,cen}$ ~9 Å) identify them as a product of an ortho-/clinoenstatite inversion. Two possibilities are conceivable for such transformations: shear stresses with >70 MPa on the (100) plane possibly due to a shock event (Coe and Kirby 1975; Buseck 1980) or rapid cooling of the protoenstatite stability field (Smith 1974). In the former case, the external stress favors the formation of clinopyroxene from orthopyroxene by introducing shear displacements along the stacking planes. In the latter case, an athermal martensitic transition is responsible for the inversion. Protoenstatite with an orthorhombic structure (Pbcn) is stable only above ~1000 °C. It is unquenchable and a rapid cooling process will produce a highly faulted clinoenstatite. A martensitic transition is reversible and a temperature increase results in the formation of orthoenstatite. For enstatite, it is difficult to distinguish between the two possibilities (shear stress or rapid cooling) for the origin of the ortho-/clinoenstatite lamellae. Also in this meteorite, a distinction with regard to both alternatives is complex, as is the formation history of this carbonaceous xenolith. Since previous studies confirmed that the Krymka parent body was shocked twice (Semenenko and Perron 1995), a rapid cooling could have been caused by a first shock

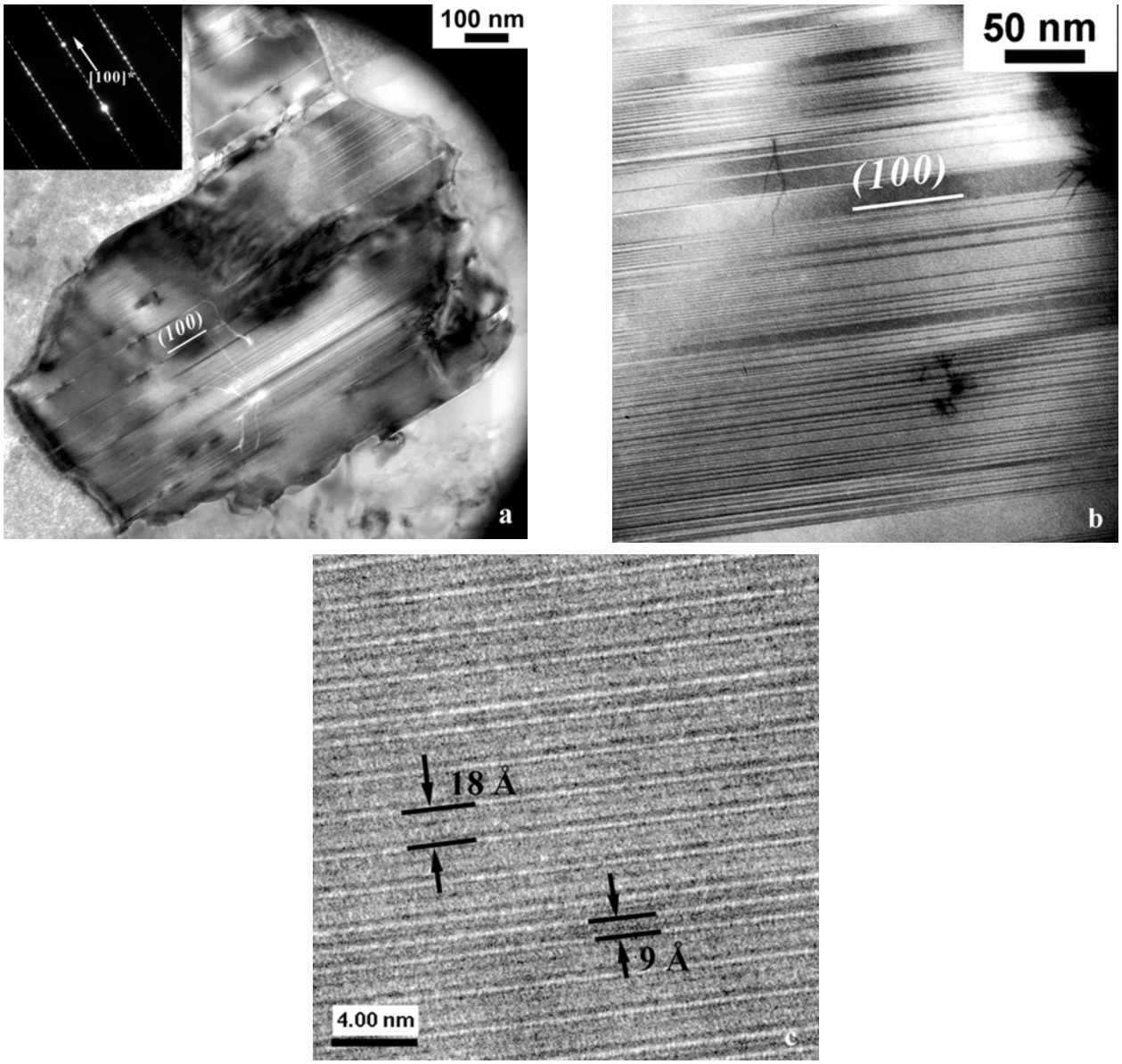


Fig. 3. a) A TEM bright field image of an ~1 µm enstatite grain. Corresponding electron diffraction pattern in the upper left corner exhibits streaking in the [100]* direction. b) An enlargement of an enstatite grain. The transformation lamellae along the (100) plane are clearly visible in this TEM bright field image. c) An HRTEM image of the enstatite in (b) that shows lamellae with lattice fringes parallel (100). Clinoenstatite can be identified by 9 Å lattice spacings, whereas the double 18 Å lattice spacings correspond to orthoenstatite.

event. This first shock event produced shock melting with temperatures higher than 1450 °C in some regions followed by quenching, and probably led to a residual temperature of nearly 500 °C within the meteorite (Semenenko et al. 1987). On the other hand, a shock-induced origin for the ortho-/clinoenstatite lamellae is also feasible, even if twinning on (100) was not observed so far. A first-assumed heavy shock event should result in dislocations in pyroxene (Langenhorst and Greshake 1999). This was not observed. Therefore, we can conclude that if the xenolith K1 was only affected by the residual temperature from the first shock, which is necessary to explain the crystalline character of graphite (as shown above), the lamellae are the result of a second, weaker shock event. However, the TEM-EDS data do not show the same variability as the SEM-EDS data. This is due to the fact that only a small region of K1 containing very few pyroxene grains was analyzed with TEM. These data are certainly not as representative as the SEM-EDS analyses.

## Graphite

Carbon occurs in the sample as well-crystallized graphite, as was proven by a diffraction pattern. Graphite in chondrites often appears as non-crystalline aggregates

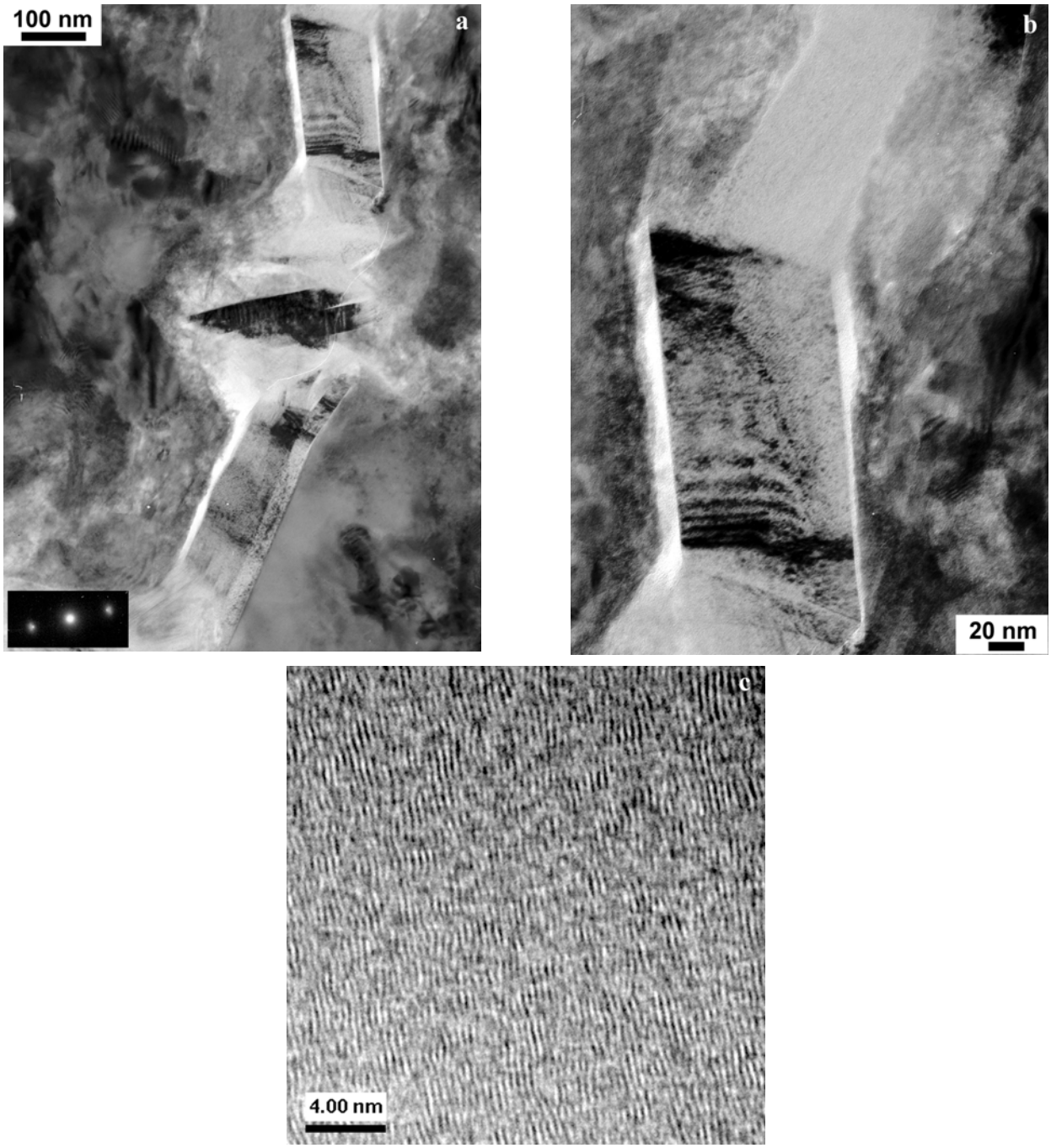


Fig. 4. a) A TEM bright field image of a graphite flake. The SAED pattern in the lower left corner shows discrete spots, indicating the crystalline character of graphite. b) Graphite showing typical kinking (TEM bright field image). c) An HRTEM image of graphite that shows short discontinuous fringes with distances of ~3.4 Å.

(Buseck and Bo-Jun 1985) or as very fine-grained crystalline aggregates (Bernatowicz et al. 1995). In addition, carbon in non-metamorphosed rocks and meteorites occurs as non-crystalline organic material. With a low-grade metamorphism, an ordering process is initiated in the carbon that ultimately yields well-crystallized graphite. That means that ordering from carbon to well-crystalline graphite increases with metamorphic grade (Buseck et al. 1987; Buseck and Bo-Jun 1985). Consequently, the degree of crystallization depends on the intensity of metamorphism and is different for various kinds of rocks. According to laboratory experiments, the first crystallization with an initial step of layer growth starts between 300 °C and 500 °C (Ruland 1968). It appears that the longer the metamorphism takes and the higher the temperature is, the better developed the crystalline character of graphite is (Buseck et al. 1987). This

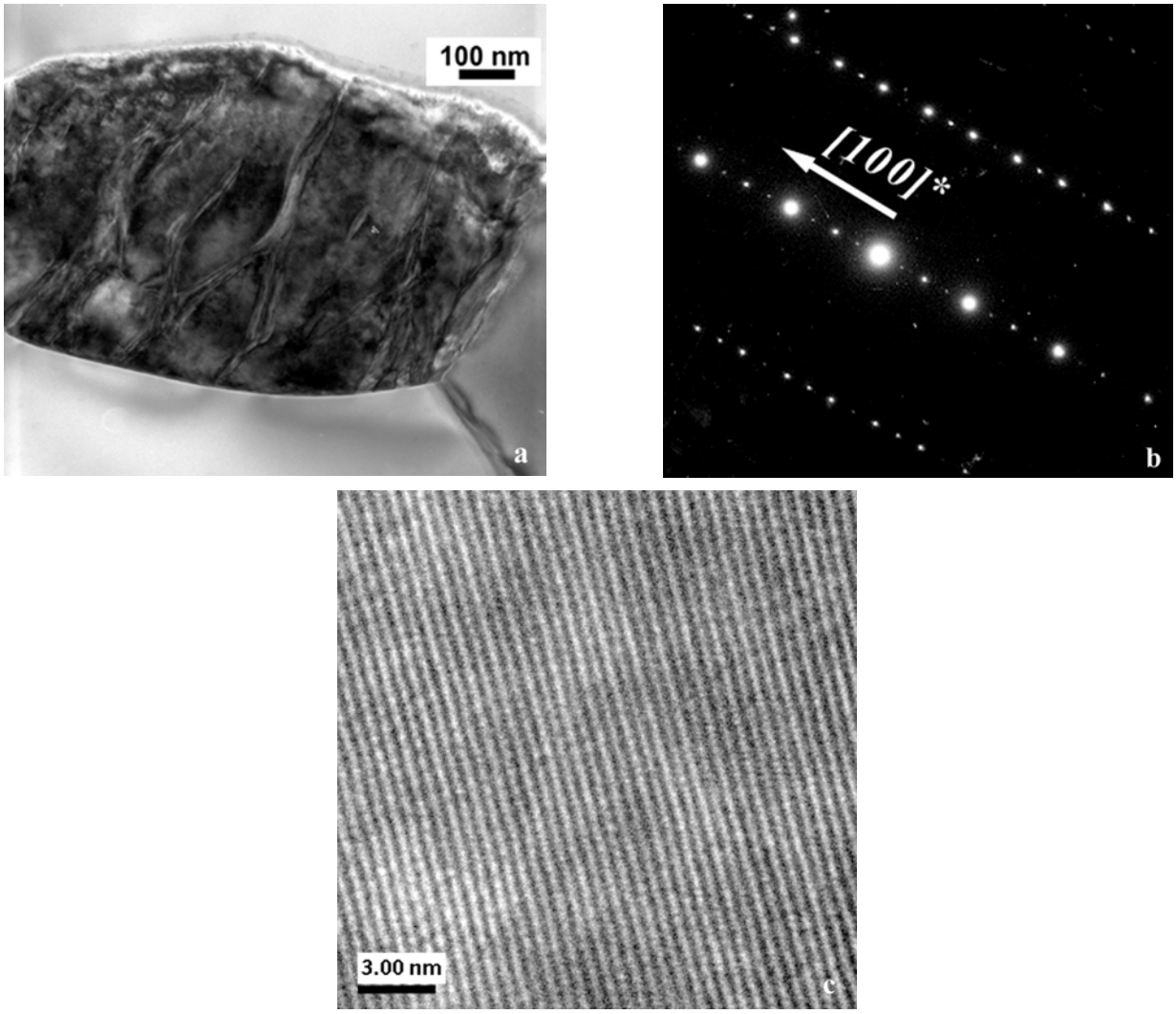


Fig. 5. a) A TEM bright field image of an ~1 µm pyrrhotite grain surrounded by olivine. b) The diffraction pattern of the 4C monoclinic pyrrhotite. Bright spots represent main reflections and small spots correspond to superstructure reflections. c) An HRTEM image of the superstructured pyrrhotite with well-ordered lattice fringes.

also fits with our HRTEM investigations where short discontinuous fringes with 3.4 Å lattice spacing are visible. With higher temperature and/or longer increasing temperature, these poorly stacked layers should result in parallel layers. Therefore the observed short layers are the result of a short, but certainly prior, thermal metamorphism. In addition, the investigated graphite shows kinking. Such a feature is established as a typical deformation mode usually found in minerals with sheet structures like graphite (Langenhorst and Deutsch 1998). Deformation, probably resulting from a shock event, was already inferred from our TEM examination of olivine and pyroxene (see above).

**FeS Phase**

The complexity of the solid solution and structure of both FeS phases, troilite (FeS) and pyrrhotite ($Fe_{1-x}S$), is certified by the extensive literature published on these phases (Buseck 1974; Carpenter and Desborough 1964; Morimoto et al. 1975; Nakazawa 1975; Posfai 1990). Nevertheless, the rare FeS phase in this section could be identified as $Fe_7S_8$ pyrrhotite despite the unspecified composition of pyrrhotite with $Fe(_{1-x})S$. In pyrrhotite, which has a metal deficient NiAs-type structure, 25% of the atomic sites may be vacant within an Fe layer. Therefore, the defective Fe layers might have four different positions. They have a high tendency to alternate from a disordered arrangement of vacancies to a state where the vacancies are completely ordered (Morimoto et al. 1975) in order to achieve a state of minimum energy. As a consequence of the NiAs-type structure, pyrrhotite exists in various structures with several different compositions. However, the structural stability limits the possible composition to >~46.5 atom% Fe (Carpenter and Desborough 1964). The structure can be described as a deformed

hexagonal closed-pack array of $S^{2-}$ ions with $Fe^{2+}$ ions in the octahedral interstices between the sulfur layers. In a solid solution, the ions are at first randomly distributed. With decreasing temperature, an ordering process takes place to reduce the stress within the crystal. The minimum internal energy is reached when the vacancies have maximum separation: the crystal has built a superstructure (a crystal builds a superstructure if the ions are ordered and not distributed randomly). Depending on the composition, numerous types of superstructures were found (Posfai and Dodony 1990), often only along a small number of lattices in the crystal. It is not clear what the most stable state for pyrrhotite is, but experimental studies show that an originally 1C-crystallized structure could rapidly form domain textures in the 4C type (Nakazawa et al. 1975). Also, 4C $Fe_7S_8$ occurs in rocks with a long cooling period with a possible intergrowth of troilite. However, the FeS phase in the sample studied is identified as a superstructure of a 4C monoclinic pyrrhotite with $Fe_7S_8$ (with $a \cong 11.9$ Å, $b \cong 6.9$ Å, and $c \cong 5.7$ Å × 4 = 4C). The HRTEM image with its well-ordered lattice fringes over a wide range suggests the existence of a superstructured crystal. This suggests a long cooling period or perhaps a long period of metamorphism above 300 °C, which is within the geothermometer range of pyrrhotite (Carpenter and Desborough 1964).

In addition, the formation of $Fe_7S_8$ is known from meteorites with a low-temperature nebular origin (Lauretta et al. 1996). This clearly supports the speculation that the high Tl/Bi ratio observed in another mysterite-bearing fragment in Krymka (Laul et al. 1973) is a product of volatile-rich, late-nebular condensate where the temperatures are already lower.

The TEM data for FeS from the carbonaceous clast are in conformity with diffraction X-ray and thermo-electromotive force (TEF) data of iron sulfide from the Krymka host (Semenenko et al. 1987). According to the latter, the average composition of the sulfide corresponds to $Fe_{0.965}S$. There are two compositional types of Krymka’s FeS. The TEF data of the first (16–32 mV/°C) correspond to that of pyrrhotite and that of the second (46–57 mV/°C) are identical to troilite from terrestrial samples. Variation of the TEF data within and among the FeS grains was interpreted as a result of a very fine intergrowth of pyrrhotite and troilite lamellae and their different quantity caused by relatively slow cooling below 140 °C (Semenenko et al. 1987).

## CONCLUSION

The detailed TEM study of the Krymka carbonaceous xenolith K1 plainly indicates that a thermal and shock metamorphism must have taken place, either on a primary body of the xenolith or on the Krymka parent body itself. The temperature for the metamorphism must have been above ~300 °C but below ~500 °C. This temperature range is within the stability field of pyrrhotite, which is necessary to produce the superstructure, and furthermore, the crystallization of carbon to graphite starts at ~300 °C metamorphic temperature. It should be mentioned that the presence of fine graphite crystals in the xenolith is the major mineralogical feature, which most clearly distinguishes them from Krymka host and from any other chondritic fine-grained material. In addition to graphite, the presence of organic compounds suggests that they are composed of not graphitized or poorly graphitized material, which most likely represents a transitional state from organic compounds to graphite caused by a metamorphic process. If we accept that the Krymka host was shocked at least twice (Semenenko and Perron 1995), the temperatures after the first shock event caused shock melting temperatures of about 1650 °C in certain regions of chondritic material and produced a residual temperature of nearly 500 °C, which led to graphite crystallization by dynamic metamorphism. At temperatures between 300 °C and 500 °C pyroxene and olivine are already in a stable state. The shock features observed in olivine, pyroxene, and graphite probably originate from excavation from the parent body or during an earlier shock event on the parent body itself.

From our TEM results, we can neither conclude nor definitely exclude an association of mysterite with comets as it was suggested by Campins and Swindle (1998).

*Acknowledgments*–The authors would like to thank F. Bartschat and U. Heitmann for technical assistance and sample preparation. We are also grateful to D. Lauretta, H. Nagahara, and one anonymous reviewer for formal and very useful reviews. This work was supported by the Deutsche Forschungsgemeinschaft (Je96/12-1) and the Deutsche Zentrum für Luft und Raumfahrt e.V. (RD-RX-50OO010-ZA).

*Editorial Handling*—Dr. Hiroko Nagahara

## REFERENCES

Bernatowicz T. J., Gibbons P. C., Amari S., and Lewis R. S. 1995. On the nature of carbon cores in interstellar graphite (abstract). 26th Lunar and Planetary Science Conference. pp. 107–108.

Buseck P. R. 1974. Electron imaging of pyrrhotite superstructures. *Science* 186:1209–1212.

Buseck P. R. and Iijima S. 1975. High-resolution electron microscopy of enstatite II: Geological application. *American Mineralogist* 60:771–784.

Buseck P. R., Nord G. L., Jr., and Veblen D. R. 1980. Subsolidus phenomena in pyroxenes. In *Pyroxenes*, edited by Prewitt C. T. Washington, D.C.: Mineralogical Society of America. pp. 117–211.

Buseck P. R., Bo-Jun H., and Keller L. P. 1987. Electron microscope investigations of the structures of annealed carbons. *Journal of Energy and Fuels* 1:105–110.

Buseck P. R. and Bo-Jun H. 1985. Conversion of carbonaceous material to graphite during metamorphism. *Geochimica et Cosmochimica Acta* 49:2003–2016.

Campins H. and Swindle T. D. 1998. Expected characteristics of

cometary meteorites. *Meteoritics & Planetary Science* 33:1201–1211.

Carpenter R. H. and Desborough G. A. 1964. Range in solid solution and structure of naturally occurring troilite and pyrrhotite. *American Mineralogist* 49:1350–1365.

Coe R. S. and Kirby S. H. 1975. The orthoenstatite to clinoenstatite transformation by shearing and reversion by annealing: Mechanism and potential applications. *Contributions to Mineralogy and Petrology* 52:29–55.

Dodony I. and Posfai M. 1990. Pyrrhotite superstructures. Part II: A TEM study of 4C and 5C structures. *European Journal of Mineralogy* 2:529–535.

Dreizin R. L. 1958. Results of studies of conditions on the fall of the Krymka stony meteorite shower. *Meteoritika* 16:105–107.

Giannuzzi L. A. and Stevie F. A. 1999. A review of focused ion beam milling techniques for TEM specimen preparation. *Micron* 30: 197–204.

Grossman L., Allen J. M., and MacPherson G. J. 1980. Electron microprobe study of a "mysterite"-bearing inclusion from the Krymka LL-chondrite. *Geochimica et Cosmochimica Acta* 44: 211–216.

Higuchi H., Ganapathy R., Morgan J. W., and Anders E. 1977. "Mysterite": A late condensate from the solar nebular. *Geochimica et Cosmochimica Acta* 41:843–852.

Hirsch P. B., Howie A., Nicholson R. B., Pashley D. W., and Whelan M. J. 1965. In *Electron microscopy of thin crystals.* London: Butterworths. 422 p.

Hutchinson D. R., Hackenberg R. E., and Shiflet G. J. 2003. A comparison of EDS microanalysis in FIB-prepared and electropolished TEM thin foils. *Ultramicroscopy* 94:37–48.

Jessberger E. K. 1999. On the elemental, isotopic, and mineralogical ingredients of ROCKY cometary particulates. *Space Science Reviews* 90:91–97.

Langenhorst F. and Deutsch A. 1998. Minerals in terrestrial impact structures and their characteristic features. *Advanced Mineralogy* 3:95–119.

Langenhorst F. and Greshake A. 1999. A transmission electron microscopy study of Chassigny: Evidence for strong shock metamorphism. *Meteoritics & Planetary Science* 34:43–48.

Langenhorst F., Boustie M., Migault A., and Romain J. P. 1999. Laser shock experiments with nanoseconds pulses: A new tool for the reproduction of shock defects in olivine. *Earth and Planetary Science Letters* 173:333–342.

Laul J. C., Ganapathy R., Anders E., and Morgan J. W. 1973. Chemical fractionations in meteorites. VI. Accretion temperatures of H, LL, and E chondrites, from abundance of volatile trace elements. *Geochimica et Cosmochimica Acta* 36: 329–357.

Lauretta D. S., Kremser D. T., and Fegley B., Jr. 1996. The rate of iron sulfide formation in the solar nebular. *Icarus* 122:288–315.

Madon M. and Poirier J. P. 1983. Transmission electron microscope observation of $\alpha$, $\beta$, and $\gamma$ $(Mg,Fe)_2SiO_4$ in shocked meteorites: Planar defects and polymorphic transitions. *Physics of the Earth and Planetary Interiors* 33:31–44.

McLaren A. C. and Etheridge M. A. 1976. A transmission electron microscope study of naturally deformed orthopyroxene. *Contributions to Mineralogy and Petrology* 57:163–177.

Müller W. F. 1993. Thermal and deformation history of the Shergotty meteorite deduced from clinopyroxene microstructure. *Geochimica et Cosmochimica Acta* 57:4311–4322.

Morimoto N., Gyobu A., Tsukuma K., and Koto K. 1975. Superstructure and nostoichiometry of intermediate pyrrhotite. *American Mineralogist* 60:240–248.

Nakazawa H., Morimoto N., and Watanabe E. 1975. Direct observation of metal vacancies by high-resolution electron microscopy. Part I: 4C type pyrrhotite ($Fe_7S_8$). *American Mineralogist* 60:359–366.

Posfai M. and Dodony I. 1990. Pyrrhotite superstructures. Part I: Fundamental structures of the NC (N = 2, 3, 4, and 5) type. *European Journal of Mineralogy* 2:525–528.

Ruland W. 1968. X-ray diffraction studies on carbon and graphite. *Chemistry and Physics of Carbon* 4:1–84.

Semenenko V. P. 1996. New data on a carbonaceous clast in the Krymka chondrite (abstract). *Meteoritics & Planetary Science* 31:A126–A127.

Semenenko V. P., Sobotovich E. V., and Tertichnaya B. V. 1987. *The meteorites of Ukraine.* Kyiv: Naukova Dumka. 217 p.

Semenenko V. P., Kolesov G. M., Samoilovich L. G., Golovko N. V., and Ljul A. Yu. 1991. Carbonaceous inclusions in the Krymka (LL3) chondrite (abstract). 22nd Lunar and Planetary Science Conference. pp. 1213–1214.

Semenenko V. P. and Perron C. 1995. Shock-melted regions in the Krymka (LL3) chondrite (abstract). *Meteoritics* 30:577.

Semenenko V. P. and Girich A. L. 1996. Graphite-containing fragments in the Krymka chondrite (abstract). *Meteoritics & Planetary Science* 31:A127.

Semenenko V. P., Bischoff A., Weber I., Perron C., and Girich 2001. Mineralogy of fine-grained material in the Krymka (LL3.1) chondrite. *Meteoritics & Planetary Science* 36:1067–1085.

Semenenko V. P., Jessberger E. K., Chaussidon M., Weber I., Stephan T., and Wies C. 2003. Carbonaceous xenoliths from the Krymka chondrite as probable cometary material (abstract). *Meteoritics & Planetary Science* 38:A10.

Semenenko V. P., Jessberger E. K., Chaussidon M., Weber I., Stephan T., and Wies C. 2005. Carbonaceous xenoliths in the Krymka LL3.1-chondrite: Mysteries and established facts. *Geochimica et Cosmochimica Acta* 69:2165–2182.

Smith J. R. 1974. Experimental study on the polymorphism of enstatite. *American Mineralogist* 59:345–352.

Stevie F. A., Vartuli C. B., Giannuzzi L. A., Shofner T. L., Brown S. R., Rossie B., Hillion F., Mills R. H., Antonell M., Irwin R. B., and Purcell B. M. 2001. Application of focused ion beam lift-out specimen preparation to TEM, SEM, STEM, AES, and SIMS analysis. *Surface and Interface Analysis* 31:345–351.

Stöffler D., Keil K., and Scott E. R. D. 1991. Shock metamorphism of ordinary chondrites. *Geochimica et Cosmochimica Acta* 55: 3845–3867.

Weisberg M. K., Zolensky M. E., and Prinz M. 1997. Fayalitic olivine in matrix of the Krymka LL3.1 chondrite: Vapor-solid growth in the solar nebular. *Meteoritics & Planetary Science* 32:791–801.

Weber I., Semenenko V. P., Stephan T., and Jessberger E. K. 2003. TEM investigation of a "mysterite" inclusion from the Krymka LL chondrite: Preliminary results (abstract #1535). 34th Lunar and Planetary Science Conference. CD-ROM.